

The Pattern of Earthquake Magnitude Clustering Based on Interevent Distance and Time

Derreck Gossett (10 * 1, Michael R. Brudzinski (10 1, Qiquan Xiong (10 2, Jesse C. Hampton (10 2

Author contributions: Conceptualization: D. Gossett, M.R. Brudzinski, Q. Xiong, J.C. Hampton . Methodology: D. Gossett, M.R. Brudzinski, Q. Xiong, J.C. Hampton . Software: D. Gossett, M.R. Brudzinski. Validation: M.R. Brudzinski, Q. Xiong, J.C. Hampton. Formal Analysis: D. Gossett, M.R. Brudzinski. Investigation: D. Gossett, M.R. Brudzinski, Q. Xiong, J.C. Hampton. Writing - Original draft: D. Gossett. Writing - Review & Editing: D. Gossett, M.R. Brudzinski, Q. Xiong, J.C. Hampton. Visualization: D. Gossett, M.R. Brudzinski, J.C. Hampton. Project administration: M.R. Brudzinski, J.C. Hampton. Funding acquisition: M.R. Brudzinski, J.C. Hampton.

Abstract The clustering of earthquake magnitudes is poorly understood compared to spatial and temporal clustering. Better understanding of correlations between earthquake magnitudes could provide insight into the mechanisms of earthquake rupture and fault interactions, and improve earthquake forecasting models. In this study we present a novel method of examining how seismic magnitude clustering occurs beyond the next event in the catalog and evolves with time and space between earthquake events. We evaluate the clustering signature over time and space using double-difference located catalogs from Southern and Northern California. The strength of magnitude clustering appears to decay linearly with distance between events and logarithmically with time. The signature persists for longer distances (more than 50 km) and times (several days) than previously thought, indicating that magnitude clustering is not driven solely by repeated rupture of an identical fault patch. The decay patterns occur in all magnitude ranges of the catalog and are demonstrated across multiple methodologies of study. These patterns are also shown to be present in laboratory rock fracture catalogs but absent in ETAS synthetic catalogs. Incorporating magnitude clustering decay patterns into earthquake forecasting models such as ETAS could improve their accuracy.

Non-technical summary An important question in seismology is whether the magnitude of an earthquake event depends on the events that preceded it. Correlations between earthquake magnitudes have been debated, and recent studies have shown statistically significant magnitude clustering correlations that could be important for earthquake forecasting as well as understanding the physics of how earthquakes rupture and interact with faults. This paper examines how statistical correlations between earthquake magnitudes evolve with time and distance between earthquake events. Our findings suggest that magnitudes are correlated over a larger time and distance between earthquake events than previously thought. Statistically significant magnitude clustering correlations are observed even after several days between earthquake events, and at distances over 50 km. These correlations are observed across all magnitude ranges in a given catalog, and have been verified using multiple techniques of correlation. We further verified our results by comparing with popular statistical models of seismicity, highlighting the validity of the methodology as well as differences between popular models used in earthquake forecasting and the patterns that are observed in real earthquake catalogs. Our results have implications for the further understanding of earthquake rupture physics, highlighting the need for additional physical models of earthquake rupture and fault interaction.

Production Editor:
Gareth Funning
Handling Editor:
Andrea Llenos
Copy & Layout Editor:
Tara Nye
Anant Hariharan

Received:
August 22, 2023
Accepted:
July 25, 2024
Published:
August 29, 2024

1 Introduction

A key aspect of earthquake sequences is the fact that they cluster in both space and time, which can inform us about the dynamics of earthquake rupture. Spatial and temporal clustering are taken into consideration in state-of-the-art earthquake forecasting models such as the Epidemic-type Aftershock Sequence (ETAS) model (Ogata and Zhuang, 2006). However, clustering of earthquake magnitudes, where the magnitude of an earthquake event is related to the magnitudes that occurred previously in the sequence, is not widely accepted such that it is not included in forecasting mod-

els like ETAS. We define magnitude clustering as statistically significant correlations between magnitudes of earthquakes in a given region and time period, beyond random occurrence and other spatiotemporal relationships such as the Gutenberg-Richter frequency-magnitude distribution (Gutenberg and Richter, 1944). More specifically, the magnitude difference between two earthquakes is smaller than would be expected from the Gutenberg-Richter frequency-magnitude distribution, based on a large number of event comparisons (catalogs on the order of 1000 events have shown statistically significant clustering) (Xiong et al., 2023). Magnitude clustering could be an important aspect of seismic sequences and their forecasting, particularly if

¹Department of Geology and Environmental Earth Science, Miami University, Oxford, OH, USA, ²Geomechanics and Damage Group (GeoD), Department of Civil and Environmental Engineering, University of Wisconsin-Madison, Madison, WI, USA

^{*}Corresponding author: gossetd@miamioh.edu

the magnitude of an earthquake correlates to a temporarily heightened risk of similar-sized events in an area. For example, this type of magnitude correlation is not included in the parameters of aftershock forecasts currently being published by the United States Geological Survey (USGS) (Hardebeck et al., 2018). Magnitude clustering could be especially important for large, destructive earthquakes that pose significant risk to human life.

The literature has documented a vigorous debate regarding magnitude clustering as a genuine physical phenomenon (e.g., Corral, 2006; Lippiello et al., 2008, 2012) or as a spurious artefact of catalog incompleteness (e.g., Davidsen and Green, 2011). Some previous studies were concerned that magnitude clustering was the effect of overall catalog incompleteness as well as shortterm aftershock incompleteness (STAI) following larger earthquakes. Recently, Xiong et al. (2023) introduced detailed analysis incorporating filters to account for catalog incompleteness and STAI across a wide range of field and laboratory catalogs. Significant clustering was shown across fault types, in tectonic and induced settings, from spatial scales of mm to 100s of km, and universally in laboratory catalogs under a shear stress condition. The results revealed statistically significant magnitude clustering in all catalogs investigated, implying some form of magnitude clustering is ubiquitous under shear conditions.

The findings of Xiong et al. (2023) were focused on demonstrating magnitude correlations for only the next event in the earthquake catalog, providing a limited exploration of the temporal and spatial scale of magnitude clustering. In the Southern California catalog, for example, the median time between an event n and the subsequent event n+1 is less than 1.5 hours. Additionally, many of the catalogs investigated did not have high precision location information. The study did note a time dependency of the clustering signature, showing the magnitude clustering signature was most prominent at time intervals less than 60 seconds in the field catalogs. Further exploring the temporal and spatial trends of magnitude clustering requires expanding the analysis beyond subsequent events to include a wider range of event separations. This study aims to build upon the research of Xiong et al. (2023) by expanding the methodology to another robust earthquake catalog with a large number of well-located events, examining the spatial and temporal characteristics of magnitude clustering. This analysis is critical to discerning the different physical mechanisms. One model proposed for magnitude clustering in the Xiong et al. (2023) study is that a particular patch of fault is re-rupturing with a similar magnitude, which would imply that magnitude clustering is confined to very small spatial differences. In this study, we present results of magnitude clustering at spatial and temporal scales inconsistent with this hypothesis alone, highlighting the need for multiple physical models of how magnitude clustering occurs.

2 Magnitude Clustering Based on Next Event Comparisons in the California Relocated Catalogs

Many prior investigations into the existence of magnitude clustering have demonstrated their techniques on the Southern California relocated catalog (Hauksson et al., 2012) (Figure 1A), because it is an ideal dataset for statistical seismology research due to its abundance of events (more than 400,000 events observed from 1981–2005) and the precision of the double-difference relocated hypocenters. In this paper, we expand the Xiong et al. (2023) method to another similar doubledifference relocated earthquake catalog in Northern California (Figure 1B). This catalog consists of more than 650,000 events recorded from 1985-2019 by the Northern California Earthquake Data Center (NCEDC) (Waldhauser and Schaff, 2007; Waldhauser, 2009). Similar to the Southern California catalog, the large number of double-difference relocated events enables more reliable statistical analyses and examination of spatial and temporal relationships of magnitude clustering.

We followed the approach of Xiong et al. (2023) in processing the seismic catalogs to account for incompleteness and test for magnitude clustering. We first utilized two standard methods of estimating the catalog magnitude of completeness via the Gutenberg-Richter frequency-magnitude distribution (Gutenberg and Richter, 1944; Mignan and Woessner, 2012) of the catalog (Figure S1). After performing this processing on the Northern California catalog, the maximum curvature method (Wiemer, 2000) produced a lower, more inclusive estimate of 1.05, whereas the *b*-value stability method (Cao and Gao, 2002; Woessner, 2005) produced a higher, more conservative estimate of 1.4. To ensure minimal effects of catalog incompleteness on our analysis, we adopted the more conservative *b*-value stability method. To correct for STAI, we follow the approach of Helmstetter (2006) of excluding events for a period after mainshock magnitudes $m \ge 6$ by relating the completeness magnitude m_c at a time $m_c(t, m)$ in days after the mainshock m by the following equation:

$$m_c(t,m) = m - 4.5 - 0.75 \log_{10}(t)$$
 (1)

We additionally excluded events separated by less than 2 minutes to address smaller mainshocks, following the approach of Xiong et al. (2023) as well as Davidsen and Green (2011). This time separation is determined by analysis of the seismic coda waveforms after larger events in the catalog, and is a conservative estimate of when the waveform returns to background levels following a large earthquake event. Small events within this 2-minute window are more likely to be missed due to the overlapping of waveforms from the larger events (Kagan, 2004; Peng et al., 2007). We also tested an alternate method of filtering the catalogs for short term incompleteness based on a ratedependent magnitude of completeness estimation using an algorithm developed by Hainzl (2016). A description of this method and results (Supplementary Figures S2 and S3) can be found in the supplementary material. The amount of magnitude clustering observed in the

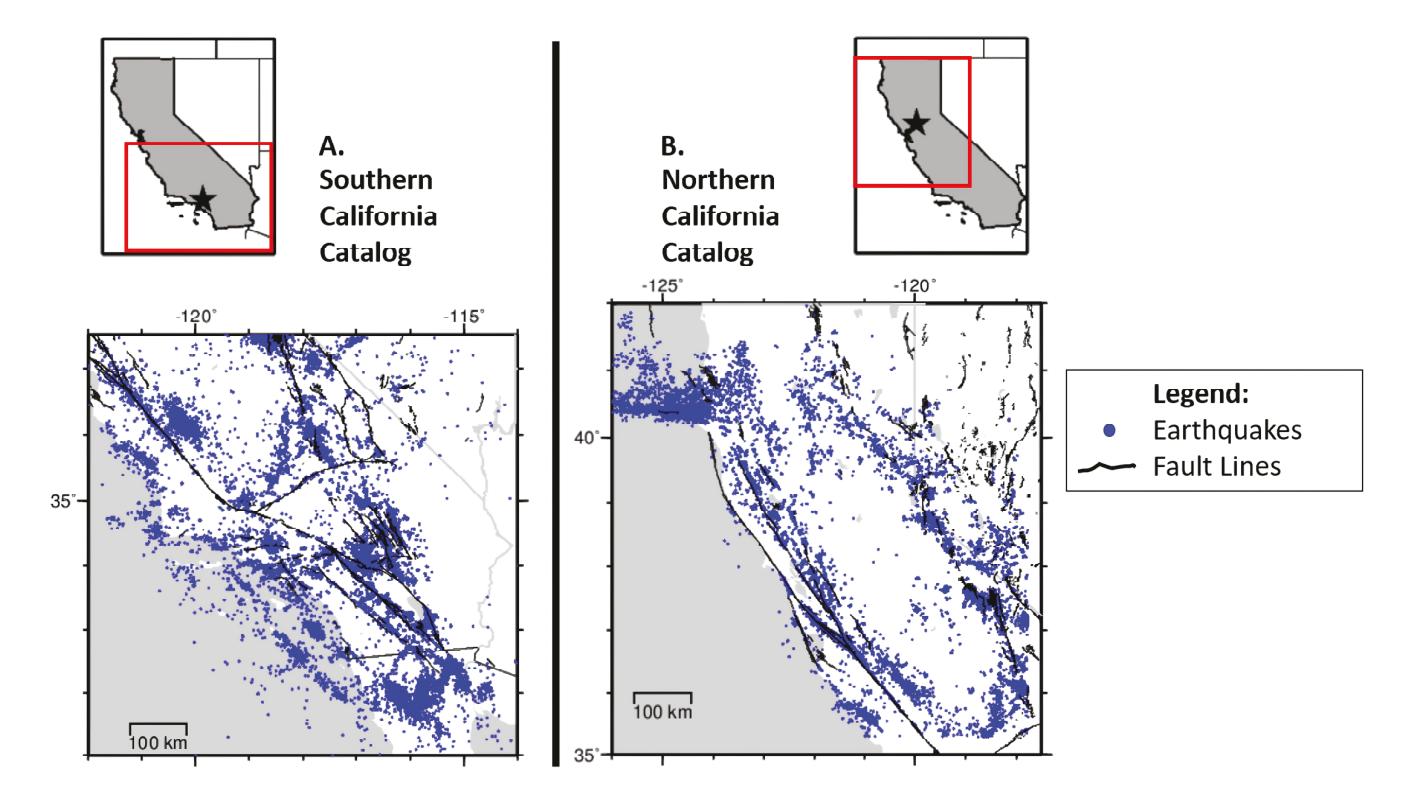


Figure 1 Maps of the Southern **A** and Northern **B** California study areas. The Southern California study area consists of 90,117 events at a m_c of \geq 2 observed between 1981 and 2005. The Northern California study area consists of 220,535 events at a m_c of \geq 1.4 observed between 1985 and 2019.

catalogs using this method is very similar to the amount observed using our methodology.

To test for statistically significant magnitude clustering, we first followed the approach of Davidsen and Green (2011) by comparing the cumulative probabilistic distribution (P) of magnitude differences (Δm) for successive events between the real catalog and a shuffled version of the catalog that randomizes the events by time, given in the equation:

$$\delta p(m_0) = P(\Delta m < m_0) - P(\Delta m^* < m_0) \tag{2}$$

where Δm^* represents the magnitude differences in the randomly shuffled version of the catalog. We also applied the filtering for catalog completeness and STAI to both the real and shuffled versions of the catalog. If no significant magnitude clustering exists, and subsequent magnitudes do not correlate with the previous magnitudes, then $\delta p(m_0)$ would not significantly deviate from zero for the entire range of magnitude differences in the x-axis of the figure. However, Figures 2A,B demonstrate that statistically significant deviations exist for smaller magnitude differences in the real catalog compared to the shuffled version, and they exist across a range of magnitude of completeness thresholds. The largest probability deviations occurred at the smaller magnitude difference values even for magnitude of completeness thresholds higher than our threshold determined by the frequency-magnitude distribution. These deviations are still observed after applying the filtering for STAI (Figures 2B,D).

These results contradict the findings of Davidsen and Green (2011), who did not observe significant probability deviations in the Southern California catalog after

filtering for STAI at their chosen catalog magnitude of completeness. However, we determine a lower magnitude of completeness for the catalog by using two different methods based on the frequency-magnitude distribution of the catalog (Wiemer, 2000; Cao and Gao, 2002; Woessner, 2005), whereas Davidsen and Green (2011) used a method based on the detection probability of the seismic stations (Schorlemmer and Woessner, 2008). The lower completeness value that we determined by multiple well-established estimation methods allows us to keep more event comparisons in the catalog, which is critical for establishing reliable statistical comparisons. Furthermore, after filtering our catalog for STAI using a different rate-dependent magnitude of completeness methodology (Hainzl, 2016), these significant deviations are still observed (see supplementary material for these results).

The decrease in the probability deviations as the catalog completeness threshold is raised indicates that some aspect of the magnitude clustering process is more prevalent at smaller magnitudes, which should be the focus of future work. We interpret the variations as real because prior work indicates that positive magnitude differences are particularly robust to incompleteness issues (van der Elst, 2021), so the fact that our magnitude clustering deviations were similar for both negative and positive magnitude differences indicates the reliability of the analysis. This result highlights that magnitude clustering is not a spurious effect due to catalog incompleteness or STAI, but a genuine physical trend in the observed Northern California catalog, consistent with the previous results of Xiong et al. (2023)

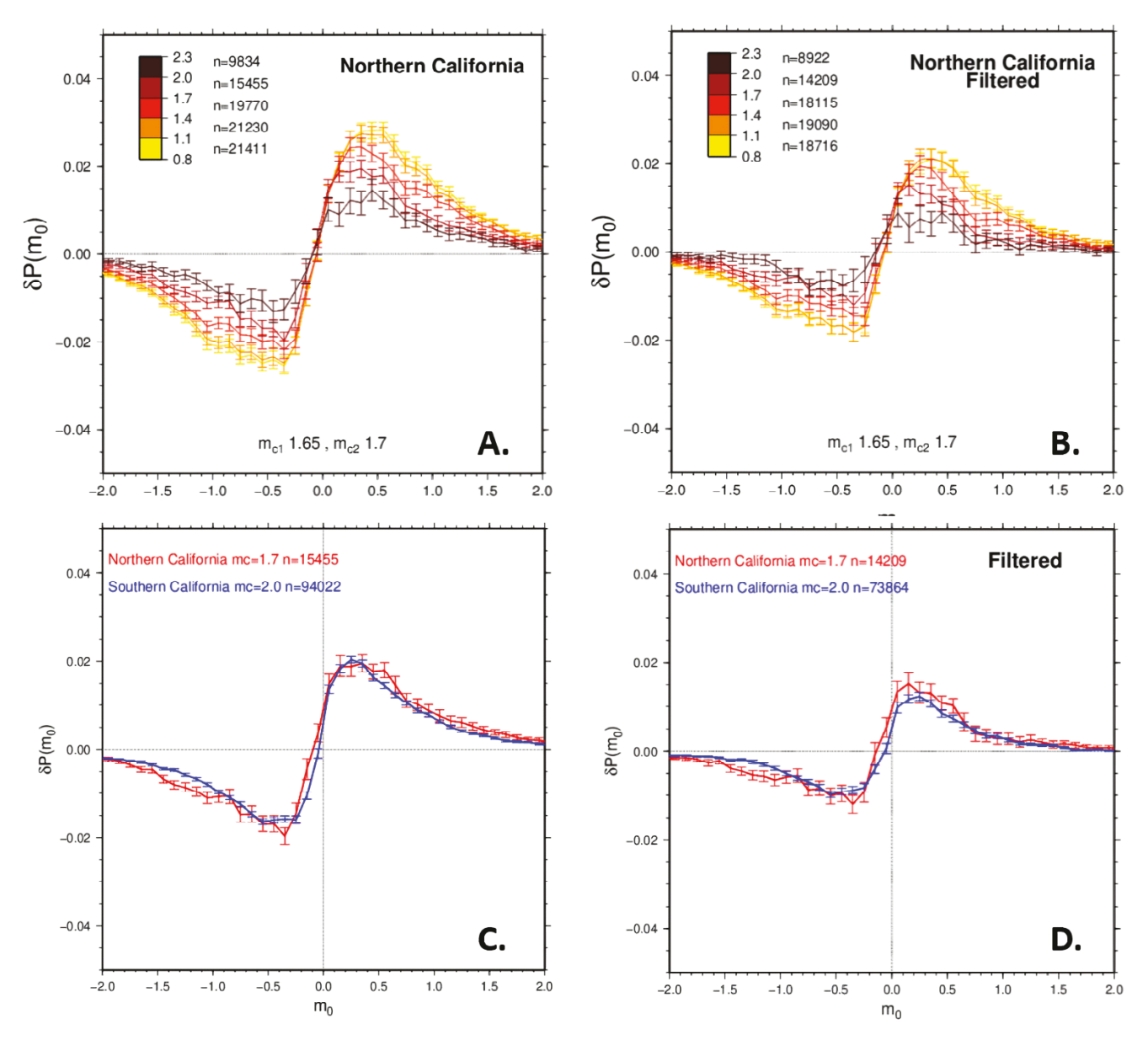


Figure 2 A Cumulative distribution of difference in probability between the observed catalog and a shuffled version, $\delta p(m_0)$ as a function of magnitude difference (m_0) for the Northern California catalog. The distribution is shown at various magnitude of completeness thresholds (corresponding to the different colored lines). $m_c =$ magnitude of completeness, n = number of events. Error bars correspond to the 1 standard deviation confidence interval (for results using a 3 standard deviation confidence interval, see Figure S5). **B** Same as **A** but after applying filters to account for catalog incompleteness and short-term aftershock incompleteness (STAI). **C** Comparison of the cumulative distribution plots of both the Northern and Southern California study areas at the respective magnitudes of completeness of each catalog. **D** same as **C** but after applying filters for incompleteness/STAI.

for the Southern California catalog (Figures 2C,D). The curves for both catalogs are a remarkable match to each other indicating some similarity in the pattern of magnitude clustering between these regions, although there are different magnitudes of completeness for these catalogs.

To investigate statistically significant magnitude clustering trends at various magnitude ranges in a given earthquake catalog, Xiong et al. (2023) introduced a novel method of comparing the magnitudes of successive earthquake events based on their respective positions in an empirical cumulative density function (ECDF) of the event magnitudes (Figure 3), a method which we adopt in this study as well. Plotting the mag-

nitudes of successive earthquake event pairs in a time-ordered sequence of the catalog allows us to visualize trends in how similar the subsequent event magnitude is to the one of the event that occurred just before it. Because the amount of events in the dataset is so large, plotting all event comparisons as individual points makes it difficult to visualize the data trends due to the density of data points. For this reason, we created bins for each 20% range of magnitudes on each axis and calculated the number of event pair data points that fall into each magnitude range bin. Heatmaps are visualized by assigning red or blue to bins based on the catalog's real difference from the mean that would be expected for a bin if there were a uniform distribution

of events across the magnitude range (total number of pairs divided by the number of bins). For comparison, randomly shuffling the time order of events before comparing the magnitudes should result in no significant deviation from a uniform distribution. This organization of magnitude range bins naturally creates a line diagonally across the middle of the plot where the range of the subsequent event magnitude is similar to that of the event before it, which is what we expect for magnitude clustering. This method is advantageous because it can demonstrate clustering behavior in different ranges of event magnitude, ensuring that potential completeness issues with the large number of small magnitude events are not causing spurious correlations of magnitudes. (For more detail regarding this ECDF method, see the associated section in the supplementary material).

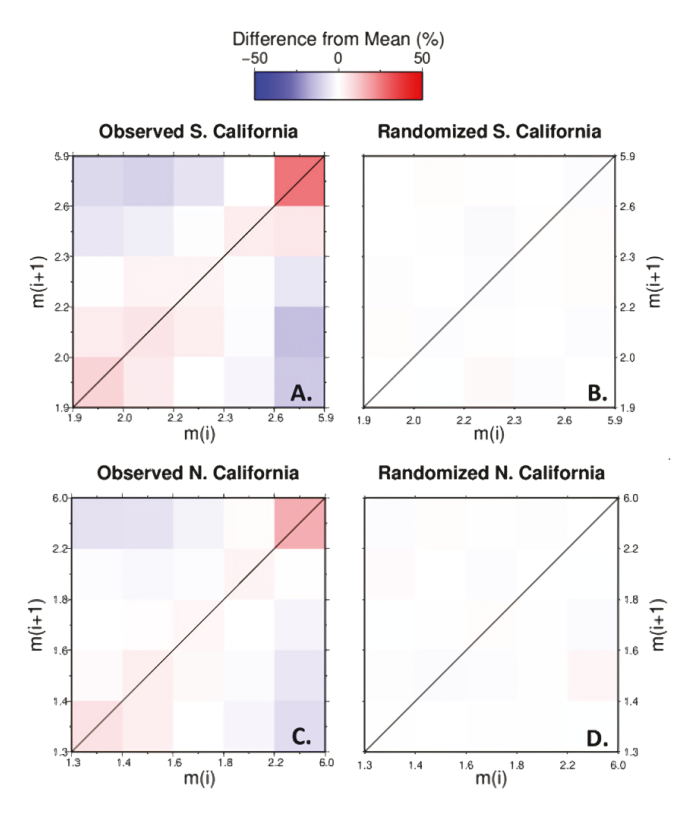


Figure 3 Empirical cumulative distribution function (ECDF) comparisons for the Southern California observed, filtered catalog **A** and a version of the catalog randomized by event time **B**. Color scale shows the number of event comparisons of the original event magnitude m(i) and subsequent event magnitudes m(i+1) that fall into each magnitude comparison bin by illustrating the difference relative to the expected mean for a bin given a uniform distribution. The diagonal line highlights subsequent events that fall into the same magnitude bin as the previous event. **C** and **D** are the same as **A** and **B** but for the Northern California catalog.

We applied the ECDF method to the STAI-filtered version of the earthquake catalogs and reported the results for comparisons of subsequent earthquake magnitudes in the 20% bins of the ECDF distribution, labeling the magnitude ranges that each quintile represents (Figures 3A,C). The resulting plot is compared to a version

of the filtered catalog that is shuffled in time to distinguish any non-random patterns in the magnitude clustering trend (Figures 3B,D). The plot highlights subsequent event magnitudes that fall into the same magnitude range bin as the events that occurred just before them (diagonal line), which is expected to have higher numbers if magnitude clustering exists. Indeed, Figure 3 shows this trend of higher amounts of subsequent earthquake events falling in the same magnitude range bin. The results demonstrate that magnitude clustering is not limited to small events, as the highest percentage increase (26% for the Southern California catalog, 17% for the Northern California catalog) occurs for the largest magnitude comparison bin. This method has a distinct advantage over the cumulative distribution approach, like that of Davidsen and Green (2011) for example, in that it shows significant magnitude correlations across the full range of catalog magnitudes, thereby refuting the idea that spurious magnitude clustering is observed due to incompleteness associated with smaller

3 Expanding Analysis beyond the Next Earthquake Event

While our previous analyses have focused on the clustering relationships among subsequent event pairs, we expanded upon this approach by examining clustering relationships among event pairs separated by up to 100 events in the time-ordered earthquake catalog. This approach enables us to analyze a wider range of interevent times and distances in a more comprehensive investigation of how the magnitude clustering signature varies with time and space.

We began by simply varying the interevent number n in the ECDF comparisons of m(i) to m(i+n) to increasing n values of 2, 10 and 100 (Figure 4). All ECDF comparisons have been filtered to correct for incompleteness and STAI via the method described in the previous section. The results indicate a decrease in the number of event comparisons that fall into similar magnitude bins as the events are further separated in number of events away from each other in the sequence. Although the clustering is about half as large at a separation of 100 events, the fact that a magnitude clustering signature persists is remarkable.

To further explore this relationship, we quantified the strength of the magnitude clustering relationship by taking the average percent difference from the mean in the magnitude bins that fall along the diagonal line of the ECDF plots for each event magnitude comparison for the m(i+n) event separations 1 to 100 (i+1,i+2,i+100). The average percent difference from mean for event comparisons with similar magnitudes is denoted as $\overline{PD}_{similar}$ and is calculated by the following equation:

$$\overline{PD}_{similar} = \frac{\overline{N}_{similar} - \overline{N}_{all\ bins}}{\overline{N}_{all\ bins}} * 100$$
 (3)

Where $\overline{N}_{similar}$ is the average number of event pairs that fall into each of the similar magnitude difference

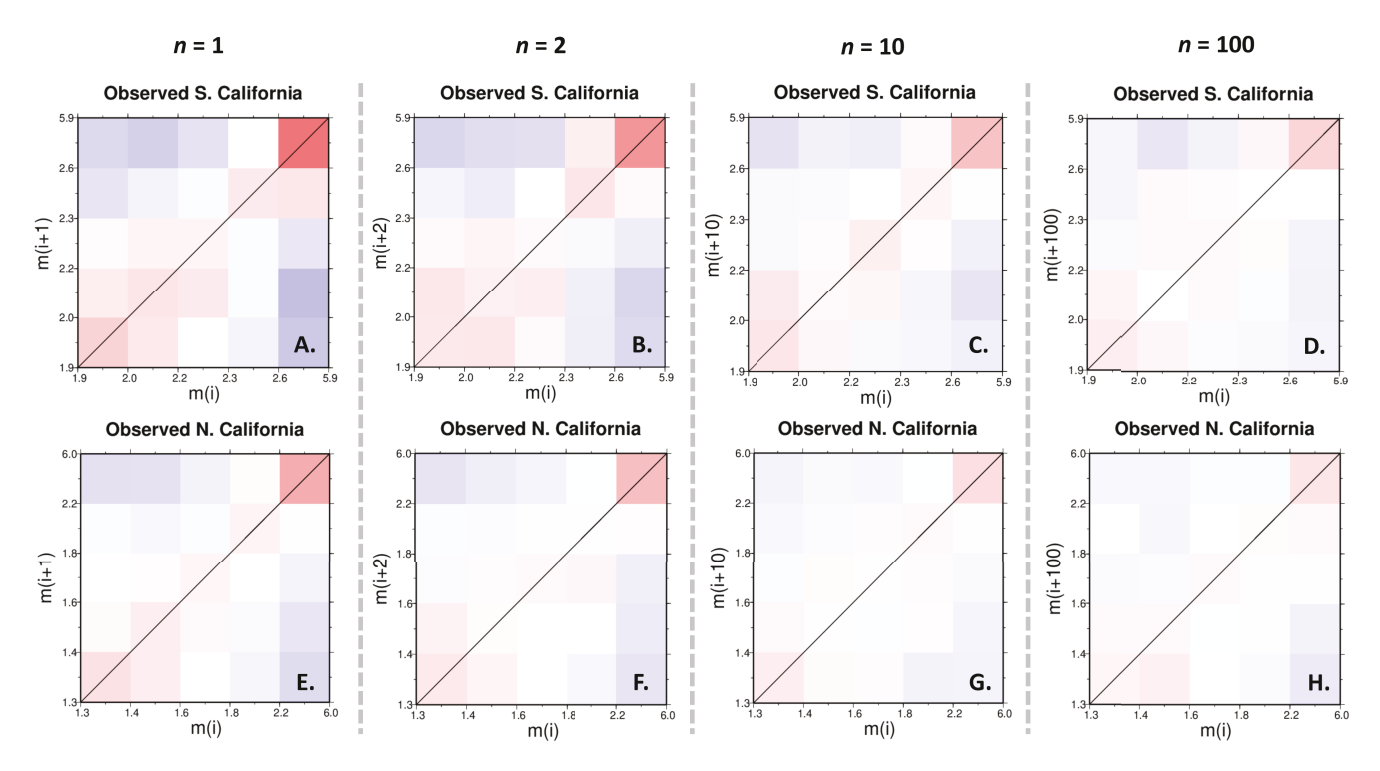


Figure 4 Empirical cumulative distribution function (ECDF) comparisons for the Southern California catalog **A-D** and Northern California catalog **E-H** for select interevent separations m(i+n). The plot illustrates a decrease in the percent difference from mean along the diagonal line of similar magnitude event comparisons with increasing interevent distance (n=1,2,10, and 100).

bins on the diagonal line in the ECDF plot, and $\overline{N}_{all\ bins}$ is the average number of event pairs in one bin based on all bins. We compared these values to those obtained by performing the same analysis on shuffled versions of the catalogs that are randomized by time. The results are plotted in Figure 5. Each plot point represents the bootstrapped mean with 1-standard deviation error bars, determined by performing 100 simulations sampling with replacement from the original sample (for both the observed and randomized versions of the data). A clear decay trend is observed in both catalogs, where the strength of the magnitude correlations decreases as the events are further separated from each other in the sequence. Conversely, there is no significant trend in the deviation from zero of the versions of the catalogs randomly shuffled by time for any event separation number. The decay observed in both catalogs is more rapid over the first few event separation numbers.

This intriguing result motivates the need to further characterize any significant patterns of magnitude clustering decay. Quantifying the relationships over space and time would be meaningful for applications of earthquake forecasting in terms of how long or expansive the clustering effect is relevant. Previous literature has suggested that magnitude clustering is most prominent over short time and distance windows, at time windows under 30 minutes (e.g., Corral, 2006; Lippiello et al., 2008; Zambrano Moreno and Davidsen, 2020) and spatial distance windows of less than 10 km (e.g., Lippiello et al., 2008). To properly evaluate these hypotheses, visualizing the change in the magnitude clustering signature over time and distance, rather than in terms of event number, will be an important first step.

4 Time Decay of Magnitude Clustering in Field Catalogs

To analyze the temporal changes in the clustering signature, we developed two distinct methodologies to see whether any temporal trends are persistent enough to help establish validity. The initial approach involved investigating the change over time observed in the $\overline{PD}_{similar}$ found in the ECDF catalog analysis. To accomplish this, we calculated interevent times for each event as compared to all following events in the filtered catalog. We subset the catalog based on interevent times into 3-hour increments ranging from 0 to 150 hours in order to visualize any change in the strength of the signature with increasing time between earthquake events over the span of a week. Considering the large spatial extent of the catalogs, and previous findings that correlations between earthquakes are more prominent in short time and space windows, we also limited the event comparisons to a maximum of 100 kilometers of interevent distance, which allows for the thickness of the seismogenic zone a modest level of fault interaction (Klinger, 2010). After imposing these time and distance restrictions, we are left with roughly 5.5 million individual event pair comparisons for the Southern California catalog, and roughly 8.5 million for the Northern California catalog. We applied the same analysis to an initially shuffled version of the catalog to assess the scale of variation expected from chance. The results are bootstrapped using the same procedure as the previously mentioned *n*-number decay analysis.

The second method employed autocorrelation, as outlined by Box et al. (2015), to investigate correlations

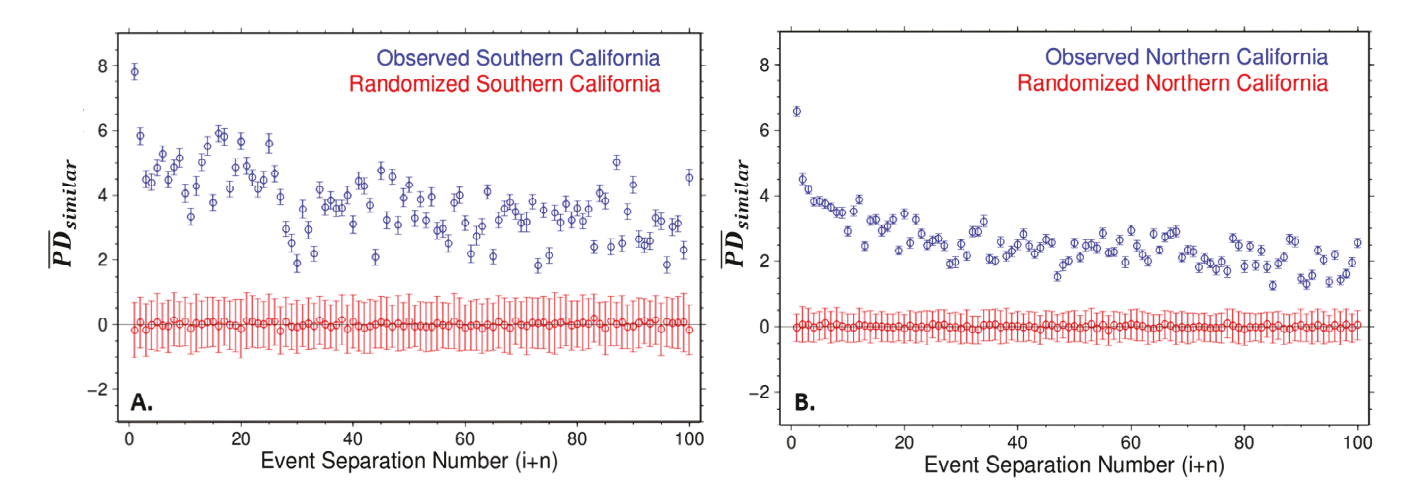


Figure 5 Strength of magnitude clustering $(\overline{PD}_{similar})$ from ECDF analysis evaluated over an increasing number of events separating the comparison for Southern California **A** and Northern California **B**. Values are bootstrapped means with 1-SD error bars from 100 simulations with 90% data resampling.

among magnitudes in the filtered catalog by treating the magnitudes over time as a time series. Autocorrelation is a widely used statistical technique that quantifies the level of randomness in a dataset at different time lags. In the absence of any non-random relationships, autocorrelation coefficients would not significantly deviate from zero across all time lags within the dataset. Conversely, if a non-random relationship exists for a particular time lag, the coefficient will exhibit a significant non-zero value. The autocorrelation coefficient is computed using the following formula:

$$R_h = C_h/C_0 \tag{4}$$

Where C_h represents the autocovariance function, given by:

$$C_{h} = 1/N \sum_{t=1}^{N-h} (Y_{t} - \overline{Y})(Y_{t+h} - \overline{Y})$$
 (5)

And C_0 represents the covariance function, given by:

$$C_h = \frac{\sum_{t=1}^{N} (Y_t - \overline{Y})^2}{N} \tag{6}$$

In our implementation of the autocorrelation function, the lag parameter h denotes the interevent time in hours between pairs of seismic events. We specifically considered lag values of 0–150 in our analysis, investigating autocorrelations between each event in the catalog and all subsequent events between 0–150 hours interevent time separation, consistent with the ECDF temporal analysis methodology.

The results of the change in the magnitude clustering signature over increasing time separations for both catalogs and methods are shown in Figure 6. In all cases, the real catalog is shown (blue) along with a comparison to a shuffled version (red). Increasing interevent time displays a decay of the signature for the real catalogs. This time decay pattern was absent in the randomly shuffled versions, wherein the signature remains near zero across all interevent time periods. The signature

in the observed catalog was largest at short time intervals (less than 20 hours), with a rapid decrease that shifts to a more gradual decrease, consistent with prior work that suggested magnitude clustering is more prominent at short time intervals. However, our short time intervals were still considerably larger (hours) than what prior work suggested (minutes). Moreover, the magnitude clustering signature persisted at a significant level above the randomly shuffled values at time frames over 100 hours of interevent time, independent of the method of time decay analysis used. This demonstrates that the magnitude relationships occur over a wider temporal range than previously thought.

The amount of magnitude clustering observed in both catalogs is similar, with some slight differences. In the ECDF analysis, the Northern California catalog shows slightly higher amounts of magnitude clustering in short time frames than the Southern California catalog, while the opposite is true for the autocorrelation. These differences are small however, and both catalogs decay to essentially the same amount of clustering in the larger time differences for both methodologies. The overall patterns of clustering decay are similar for both the ECDF and autocorrelation methods, but with a more pronounced rapid decrease in the smaller time differences for the Northern California catalog observed across both methodologies. The decay curves for both methods were rescaled via min-max normalization in Supplementary Figure S6 for a more direct visualization of the similarities of both curves.

5 Distance Decay of Magnitude Clustering in Field Catalogs

To gain further insight into the statistical patterns of seismic magnitude clustering, we also sought to characterize the change in the signature over varying spatial scales. Given that autocorrelation is designed to address time series data, we did not find it to be directly applicable to distance analysis. Consequently, we focused on developing an ECDF analysis method akin to

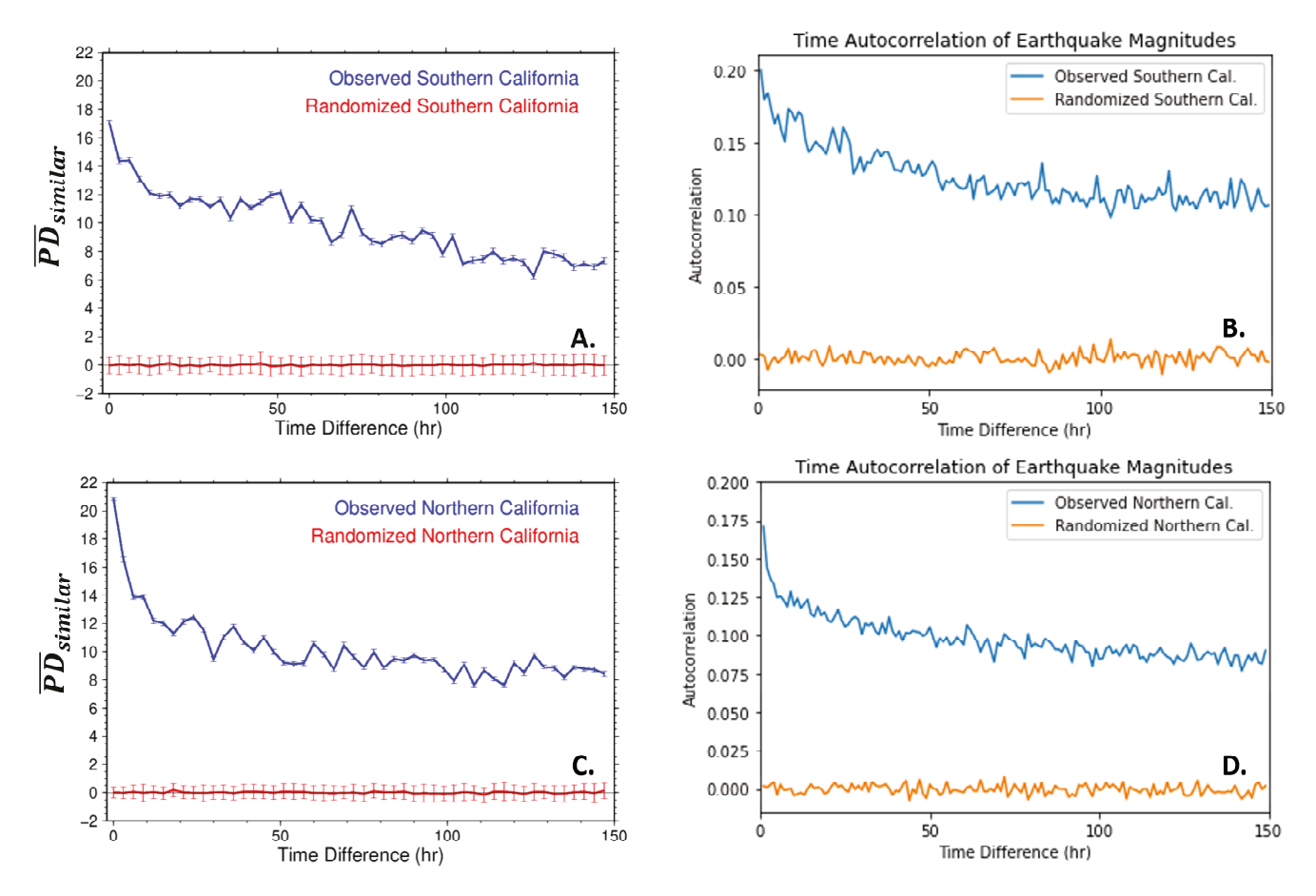
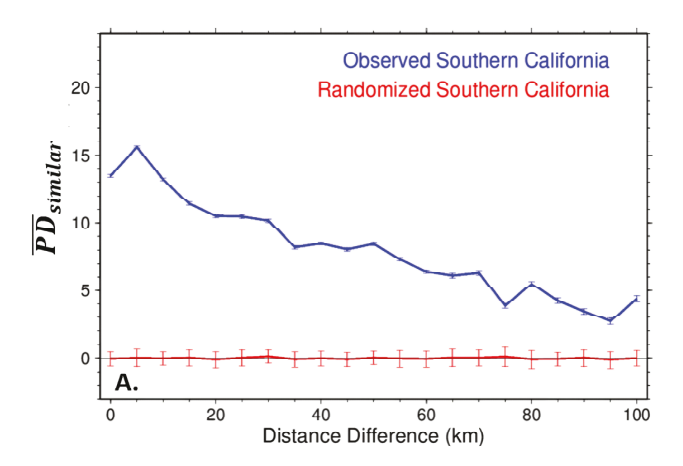


Figure 6 Time decay of magnitude clustering for both California catalogs. **A** and **C** show $\overline{PD}_{similar}$ for event comparisons separated into subcatalogs of increasing interevent time ranges at 3-hour intervals from 0–150 hours. Values for ECDF plots are bootstrapped means with 1-SD error bars from 100 simulations with 90% data resampling. **B** and **D** show the autocorrelation coefficients over increasing interevent time for a correlation of event magnitudes with each event in the catalog compared to all subsequent events separated from 0–150 hours.

the one employed for the time decay investigation. In this case, we segmented the filtered catalog based on increasing interevent distance, organizing the catalog into 5-kilometer increments ranging from 0 to 100 km. We also imposed an interevent time restriction, limiting the comparison to events separated from 0–150 hours. The $\overline{P}\overline{D}_{similar}$ is calculated for all event comparisons in each interevent distance interval.

Figure 7 presents the results of the analysis, showing the changes in the magnitude clustering signature with increasing interevent distance for both catalogs. The corresponding time-shuffled versions of the catalogs are also shown for reference, as they remain around 0 similar to the time separation analysis. There is a clear decay trend for the observed catalog as interevent distance increases. The maximum amount of magnitude clustering is similar for both catalogs ($\overline{PD}_{similar}$ just over 15%), and the maximum values are observed at short interevent distance intervals (0-10 km). The overall shape of the decay pattern is similar for both catalogs, and notably it appears to be more linear than the time decay trends. This is confirmed via regression modeling (Table S1), which shows that the linear trend has a higher statistical significance compared to logarithmic or power-law that best fit the temporal decay. The lack of similarity in these trends for space and

time indicates that the pair of patterns are not simply due to correlations between interevent times and distances. The linear decay with distance is unexpected considering one of the more prominent spatial decay patterns is that the linear density of aftershocks follows a power-law decay with distance (Brodsky, 2011; Moradpour et al., 2014). Moreover, the elevated magnitude clustering signature does not decay back into the range of shuffled catalog values until ~ 60 km for Northern California and over 100 km for Southern California. The persistence of magnitude clustering out to such large distances implies that it is not due to repeated rupture of the same event patch—which indicates that another model, or multiple models that could include the repeated rupture of the same event patch, are necessary to describe this behavior. Developing and testing physical models that can account for the linear decay of magnitude clustering with distance should be a focus of future work given that power law decay is a hallmark of spatial clustering of seismicity (Richards-Dinger et al., 2010).



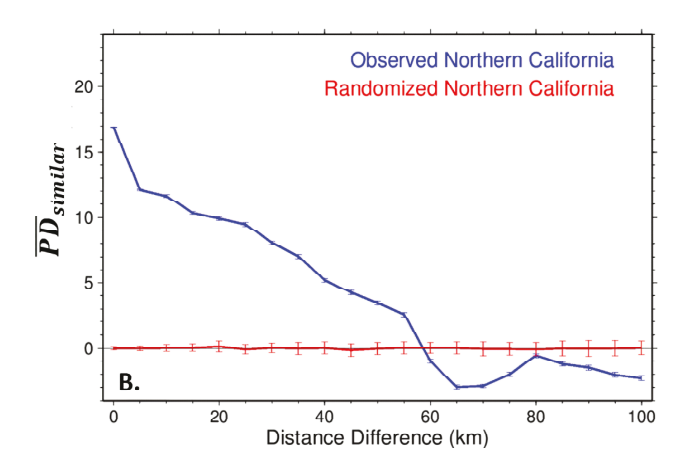


Figure 7 Distance decay of magnitude clustering for the Southern **A** and Northern **B** California catalogs. Plots show the $\overline{PD}_{similar}$ for event comparisons separated into subcatalogs of increasing interevent distance ranges at 5-kilometer intervals from 0–100 kilometers. Values are bootstrapped means with 1-SD error bars from 100 simulations with 90% data resampling.

6 Time and Distance Decay of Magnitude Clustering in Field Catalogs

To explore whether the different spatial and temporal decay patterns influence each other, we evaluated the degree of magnitude clustering for a series of event comparison groups with incrementally varying space and time differences. Figure 8 shows the results of this analysis with the space and time differences shown on the two horizontal axes and the degree of magnitude clustering shown on the vertical axes (emphasized with the color scale). To put this in context, Figure 6 represents combining all of the event comparisons for various distances into a single group to evaluate the overall temporal decay and Figure 7 represents the equivalent combination for the various times to evaluate the spatial decay. Figure 8 illustrates that the overall pattern of linear decay of magnitude clustering with distance persists for nearly all of the time groups, although there are increased fluctuations due to the smaller number of event pairs in each time and space subset. The logarithmic decay in magnitude clustering with time persists for many of the various distance groups, but appears to become diminished in the larger distance groups, particularly in Northern California when the $\overline{PD}_{similar}$ values approach 0.

7 Decay Patterns in Laboratory Catalogs

Based on the recent finding that significant magnitude clustering occurs in a variety of laboratory experimental catalogs similar to the patterns observed in field-level earthquake catalogs, we sought to investigate whether similar time and distance decay patterns are also present in laboratory catalogs. We applied the time and distance decay analysis to a mixed mode bending laboratory experimental catalog containing 4,312 acoustic emission events shown to contain significant magnitude clustering by Xiong et al. (2023). Note that this catalog is one example of the catalogs we have investigated for validating the magnitude clustering in

laboratory rock mechanics tests (Hampton et al., 2019; Lin et al., 2014, 2019b,a; Pan et al., 2018; Xiong and Hampton, 2020, 2021). Those catalogs were compiled from the rock mechanics tests conducted at different institutes, by different experimentalists, and acquired by different sensor and data acquisition assemblies, while consistent results about the magnitude clustering pattern were obtained (Xiong et al., 2023).

The laboratory catalog differs from the field earthquake catalogs in the incompleteness considerations. In laboratory conditions, the loading rate can be controlled, while in tectonic conditions the loading cannot. The commensurate control on seismicity rates minimizes the issues from short-term shaking that prevents recording of small subsequent events. As such, the primary concern regarding incompleteness is the limitation of detecting lower magnitude events. We filtered the catalog accounting for this incompleteness based on the deviation from power-law of the frequencymagnitude distribution, similar to the field catalogs. The deadtime for the acoustic emission data acquisition system was at the order of the data sample rate, and the maximum signal/hit rate for this test was far below the saturation level. As a result, the STAI is not a concern for the laboratory catalog being analyzed in this study.

The results displayed in Figures 9A,B for the magnitude clustering time decay in the laboratory catalog are almost entirely above the background variation established from the shuffled catalog. The $\overline{PD}_{similar}$ values appear to be $\sim 5\%$ for most of the range of time values, with no discernable decay pattern over the time frame analyzed. For the spatial analysis in Figure 9C, the $\overline{PD}_{similar}$ value is $\sim 10\%$ for the shortest distance and decays roughly linearly to background values by the 10-15 mm distance range. The spatial decay pattern appears slightly less linear than for the field catalogs, but would be linear without the value at the smallest spatial separation, where the source location error estimations for laboratory catalogs can be around 3 mm crossing different experimentalists' tests (Goebel et al., 2012; Lei, 2003; McLaskey and Lockner, 2018; Xiong and Hampton, 2020). The temporal analysis however, is of no ap-

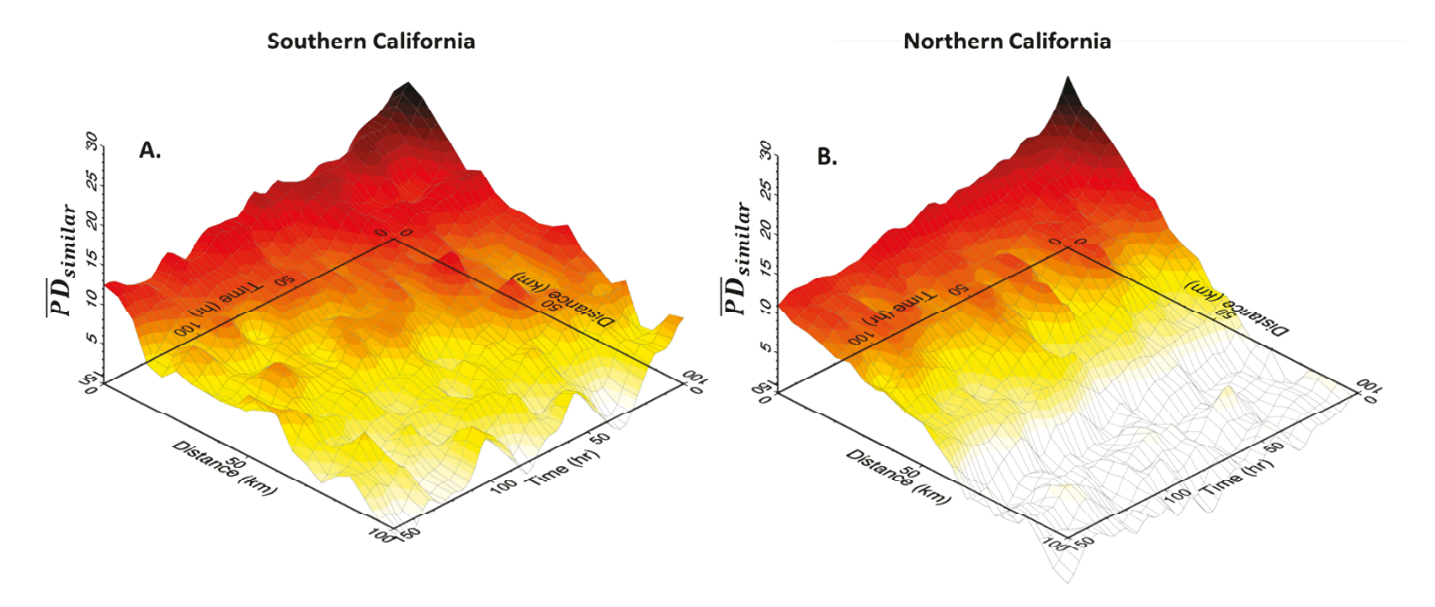


Figure 8 Spatiotemporal decay of magnitude clustering for the Southern **A** and Northern **B** California catalogs. Plots show the $\overline{PD}_{similar}$ for event comparisons of both increasing interevent distance and time on the two horizontal axes.

parent decay pattern. Such observations should be attributable to the fact that the temporal energy input for driving the laboratory rock fracture process was well-controlled under laboratory setting, while the analogue energy driving the tectonic movement was not controllable.

8 Lack of Time and Distance Decay in ETAS Simulated Catalogs

To help confirm the validity of the observed time and distance decay patterns, we can also apply our analytical approach to catalogs generated using the Epidemic-type Aftershock Sequence (ETAS) Model. The ETAS model is one of the most widely used earthquake forecasting models, utilizing spatial and temporal earthquake clustering relationships to quantify seismic activity in an area over time. It considers previous seismicity and these spatiotemporal clustering patterns to build a robust forecasting model establishing the earthquake rate as follows:

$$l(t, x, y) = \mu \sum_{i: t_i < t} g(t - t_i, x - x_i, y - y_i)$$
 (7)

Where μ is the background seismicity rate and g is the aftershock triggering rate of events triggered by an event of magnitude m at a time difference Δt and spatial distance $(\Delta x, \Delta y)$ (Mizrahi et al., 2021), given by:

$$\frac{k_0*e^{a(m-m_{ref})}}{\frac{(\Delta t+c)^{1+\omega}}{e^{\frac{-\Delta t}{2}}}*((\Delta x^2+\Delta y^2)+d*e^{\gamma(m-m_{ref})})^{1+\rho}} \tag{8}$$

as outlined in Nandan et al. (2017). To calibrate the ETAS model for use in forecasting, the background rate parameter and all parameters that define the aftershock triggering must be calibrated, usually done by utilization of the Expectation Maximization Algorithm fit to the region and time frame of seismicity studied (Veen

and Schoenberg, 2008). By design, the ETAS model considers the event magnitudes in a sequence to be independent of each other, so the time and distance patterns of magnitude clustering we observe in the real catalogs should be absent in the ETAS synthetic catalogs. If our analytical approach is flawed, it could force trivial observations of magnitude clustering when applied to ETAS synthetic catalogs.

We created synthetic ETAS catalogs fit to parameters found for Northern and Southern California using the approach of Mizrahi et al. (2021). These ETAS catalogs are simulated over the same time frame and study areas as the two California catalogs and consist of 429,607 events for the Southern California ETAS catalog and 511,973 events for the Northern California ETAS catalog. Both synthetic catalogs are filtered for catalog incompleteness and STAI in the same way as the real catalogs. Information on what each ETAS parameter represents, and the parameter value chosen based on a fit of the California catalogs, see Supplementary Table S2. Using our ECDF approach, we found no evidence of overall magnitude clustering in these catalogs (Figure S7) after applying our completeness and STAI filtering methods. Nevertheless, we went ahead with applying our time and distance decay plotting methodology to investigate whether there were temporal or spatial changes in the strength of magnitude clustering. The results shown in Figure 10 demonstrate that the ETAS models constructed from both catalogs have no signature of increased magnitude clustering at small time or distance separations. To further explore issues with catalog incompleteness we created several versions of the ETAS catalog with incompleteness added by artificially removing smaller magnitude events from the catalog (Supplementary Figures S8-S9). Introducing catalog incompleteness did not artificially produce any magnitude clustering, regardless of whether it is designed to reproduce overall catalog incompleteness or STAI. This highlights the difference between ETAS forecast-

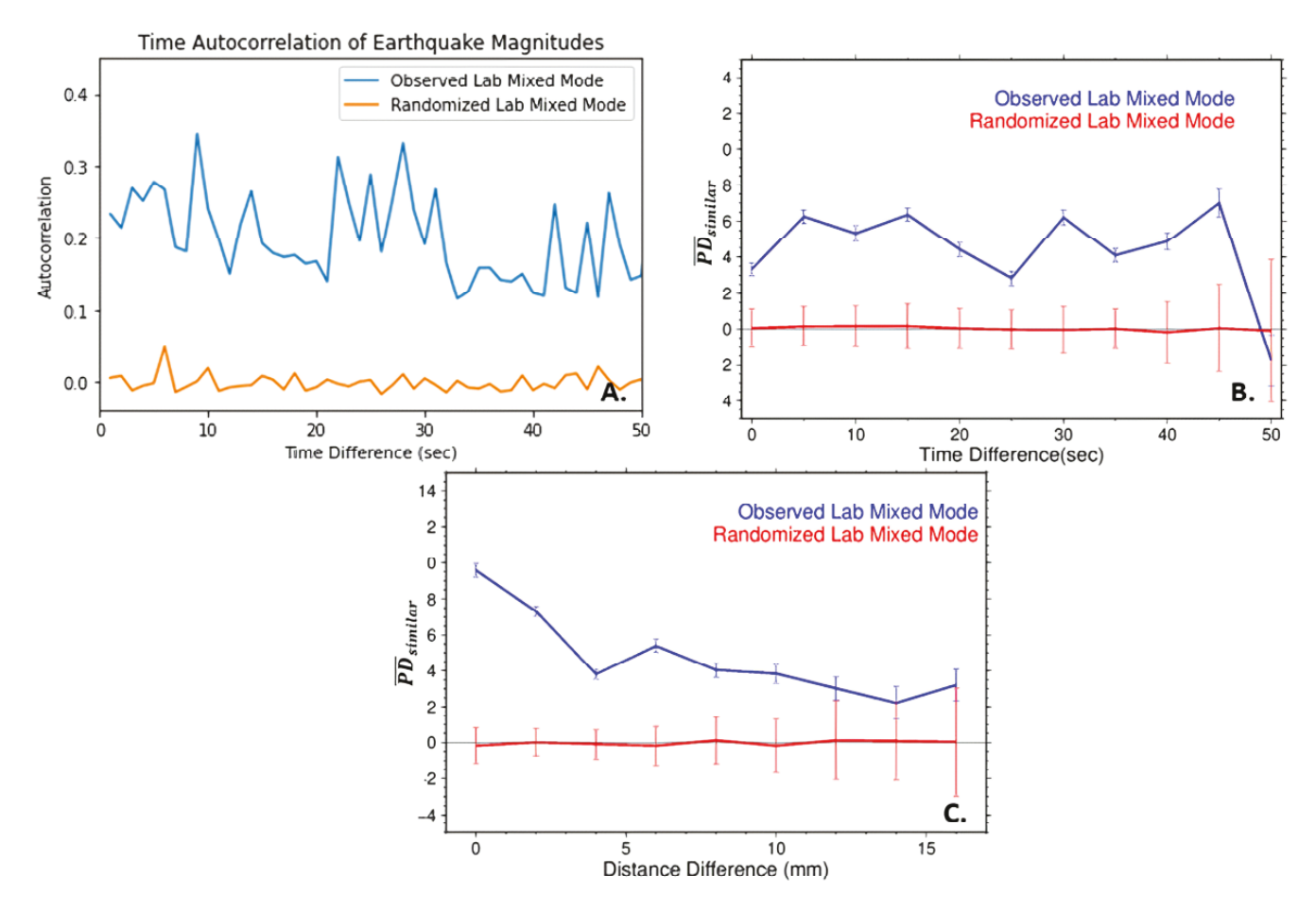


Figure 9 Magnitude clustering decay plots for the laboratory mixed mode bending catalog. **A** autocorrelation time decay, **B** ECDF time decay, **C** ECDF distance decay. n=4,312 events. Values for ECDF plots are bootstrapped means with 1-SD error bars from 100 simulations with 90% data resampling.

ing and real catalogs, as well as demonstrating that our methodology does not force spurious observations of magnitude clustering. Furthermore, our results suggest that incorporation of magnitude clustering into the ETAS model can improve the accuracy of forecasting by more accurately simulating the observed seismicity patterns.

9 Variations in Time and Distance Decay Patterns for Different Magnitude Ranges

One feature of the ECDF plots (Figures 3 and 4) is the differing \overline{PD} values along the diagonal line that highlights magnitude bins where subsequent events fall into the same magnitude bin as the previous event. The \overline{PD} values are generally highest in the largest magnitude quintile bin, followed by the lowest quintile bin. The three bins in the middle generally have lower \overline{PD} values than the upper and lower quintiles. Considering this, we sought to investigate whether the same patterns of time and distance decay are observed throughout the catalog, and not just driven by the upper or lower magnitude quintiles. To accomplish this, we created split versions of the time and distance decay plots separated into three groups based on magnitude quintiles. The chosen ranges for the three groups were 0-20%, 20-80%, and 80-100% (corresponding to the lower left, middle three,

and upper right magnitude range bins along the diagonal line in the ECDF plots). Results of this analysis are shown in Figure 11.

We first examine the time decay patterns (Figures 11A,B). Note that the data in these time decay plots have been converted to a log-log form to more easily visualize any variations in the logarithmic decay between the three magnitude bin ranges. While the overall magnitude of the \overline{PD} values (and thus the overall amount of magnitude clustering observed) does change over the three magnitude bin ranges, the logarithmic decay pattern is observed in all three ranges, implying that the time decay relationship is robust over all ranges of magnitude in the catalogs. The slope of the time decay patterns is very similar in each range, especially for the Northern California catalog. While there is more variation in the slopes for the Southern California data, the slopes are still very similar overall.

Similar results can be seen in the distance decay patterns, (Figures 11C,D), with a difference in the overall magnitude of the \overline{PD} values over different magnitude ranges, but with a robust (and linear) pattern of decay in the magnitude clustering signature. However, the slope of the spatial decay pattern in the largest magnitude range bin (80-100%) is significantly steeper than the slope of the other two ranges observed. The difference in the steepness of the distance decay slopes can likely be explained mathematically by observing the initial

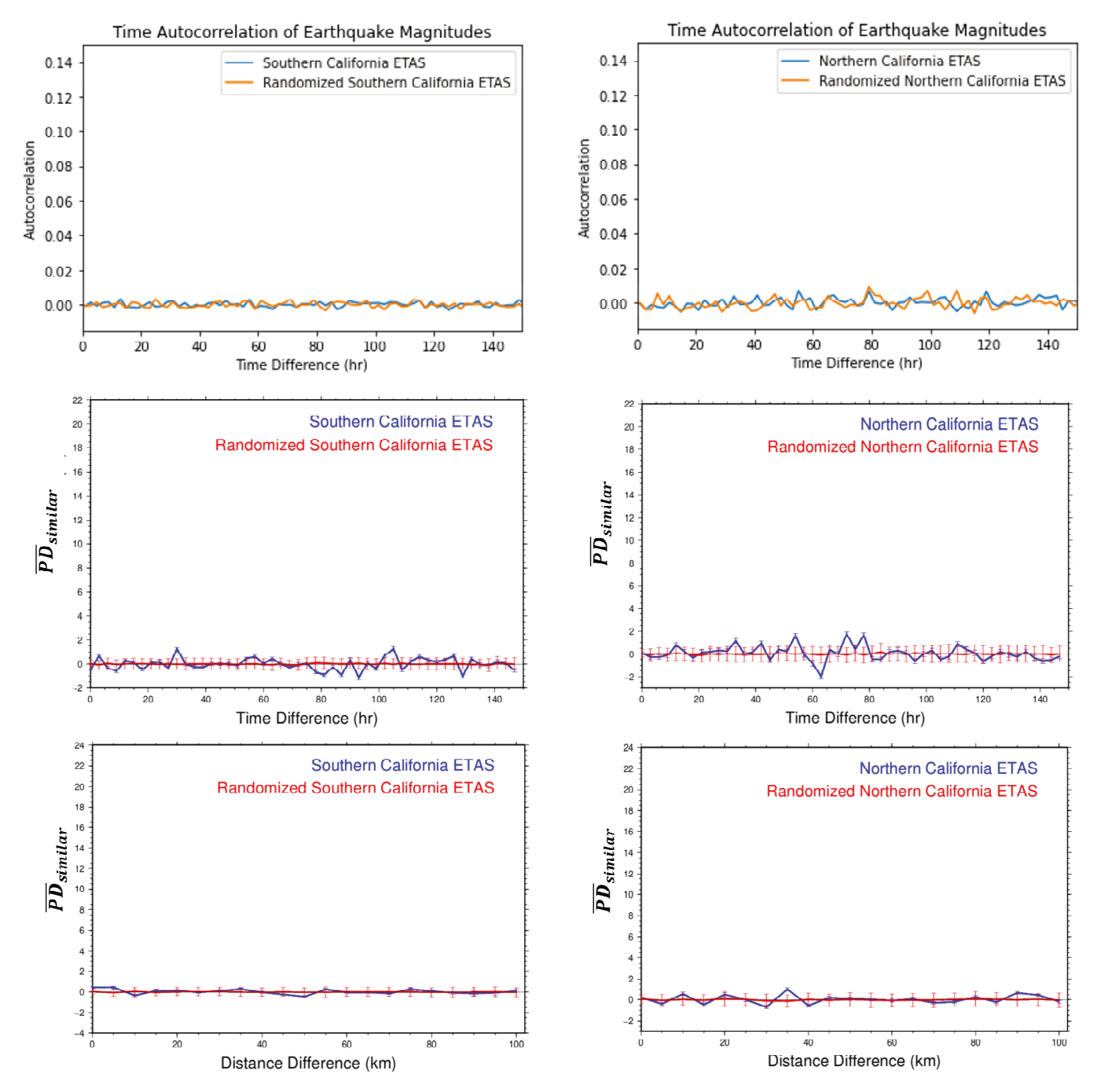


Figure 10 Time and distance decay plots for ETAS catalogs fit to the Southern **A**, **C**, **E** and Northern **B**, **D**, **F** California catalogs. Values for ECDF plots are bootstrapped means with 1-SD error bars from 100 simulations with 90% data resampling.

strength of the magnitude clustering value for each of the different magnitude ranges. There is a clearly similar linear decay for each of the magnitude ranges. However, since the initial strength of the magnitude clustering value in the highest magnitude range is much larger compared to the other two ranges, this would naturally lead to a steeper decay slope mathematically if it decays in a similar fashion to other two ranges. To decay to a similar value of magnitude clustering observations at a distance where we believe the distance is likely too large for magnitudes to significantly cluster, it naturally must decay at a steeper slope from its initially higher value. The time decay slopes don't show this difference due to being presented in a log-log space. Overall, both temporal and spatial decay curves show a robust decay pattern

across all different magnitude ranges in the catalogs.

10 Conclusions

We examined seismic magnitude clustering beyond just the next event in a catalog, comparing the magnitude of each event to all subsequent events separated by ≤ 150 hours and 100 km. This method allows for the analysis of a wider range of interevent times and distances to understand how the magnitude clustering signature varies with time and space. We demonstrated that while the magnitude clustering signature decreases with further interevent time and distance separation, remarkably the signature persists at much longer times and further distances than previously thought. The mag-

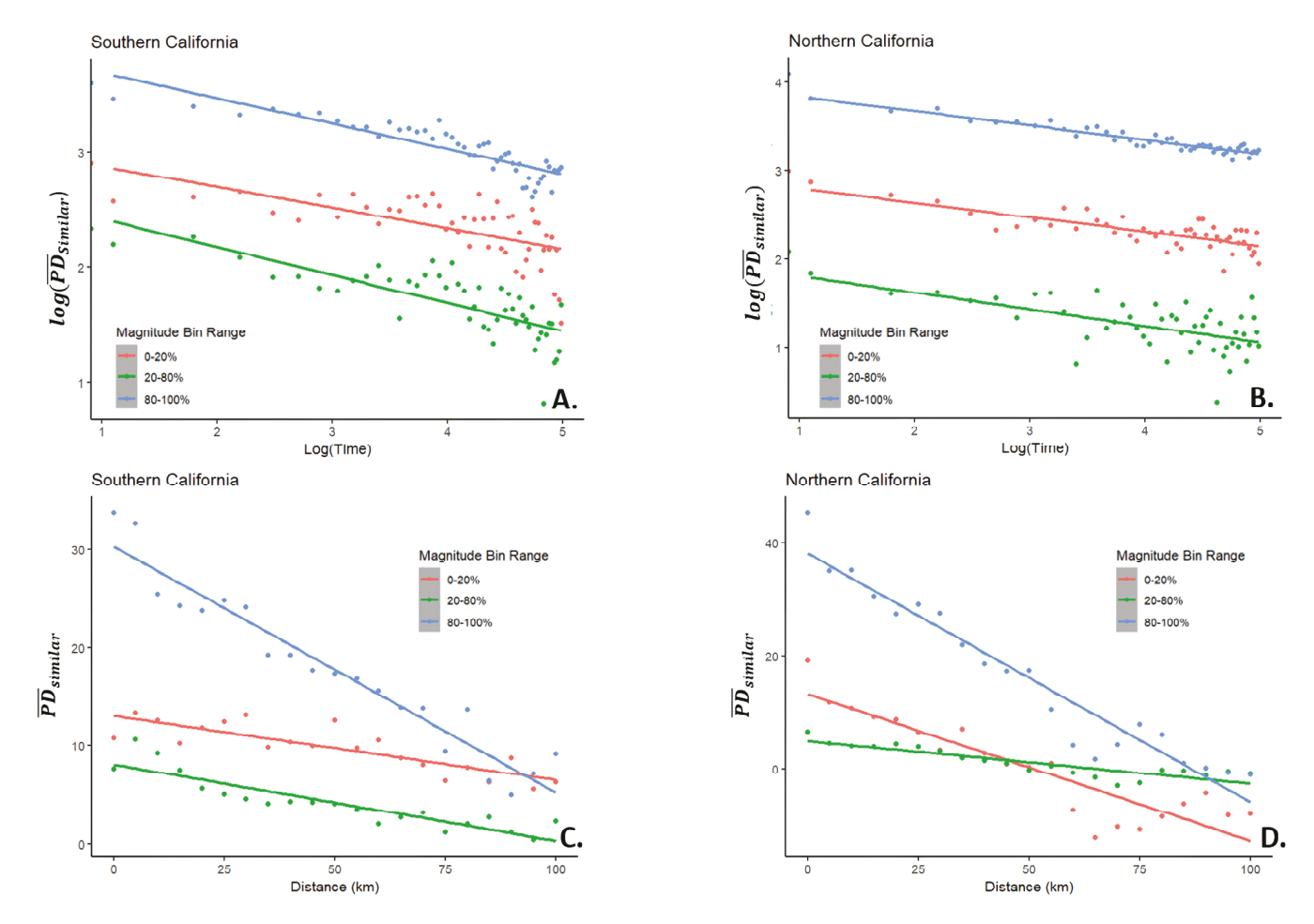


Figure 11 ECDF decay plots split by magnitude range bins. **A** Southern California time decay, **B** Northern California time decay, **C** Southern California distance decay, **D** Northern California distance decay.

nitude clustering signature remains significant at interevent times of several days, and at interevent distances of more than 50 km. The laboratory catalog results show that these time and distance decay patterns also exist at the distance scales of mm and time scales of seconds to minutes, but the trends are more muted at these scales. The decay patterns of the magnitude clustering signature are distinct and consistent across multiple methodologies of analysis, and are not limited to largest or smallest magnitudes. The strength of magnitude clustering appears to follow a linear decay with increasing distance while following a logarithmic decay with increasing time, indicating the patterns are not simply due to correlations between interevent times and distances. The persistence of the magnitude clustering signature beyond 50 km indicates that magnitude clustering is not driven solely by repeated rupture of an identical fault patch. Additional physical models are needed in conjunction with those established in the literature to fully explain the observed clustering patterns. We utilized ETAS synthetic modeling to confirm the validity of our analysis, demonstrating that our approach does not force trivial magnitude clustering. Furthermore, the absence of magnitude clustering decay patterns in ETAS synthetic catalogs highlights the difference between synthetic and real catalogs, suggesting that incorporation of magnitude clustering into forecasting models would improve their accuracy.

Acknowledgements

We sincerely thank the reviewers and the journal editor, Andrea Llenos, for their helpful comments and suggestions that helped improve this study. We would also like to thank Ellie Johnson for checking/revising the code and for her helpful suggestions on improvements to the manuscript text.

Data and code availability

The code used for this study can be found in the following repository: https://zenodo.org/records/12565430. Datasets used in this study are open-source and have been cited in references where applicable. Versions of the earthquake catalog datasets formatted for use with this code have also been included in the repository. A list of data source locations can also be found in the repository linked above.

Competing interests

The authors declare no competing interests.

References

Box, G. E. P., Jenkins, G. M., Reinsel, G. C., and Ljung, G. M. *Time series analysis: Forecasting and control.* Wiley, 2015.

- Brodsky, E. E. The spatial density of foreshocks: THE SPATIAL DEN-SITY OF FORESHOCKS. *Geophysical Research Letters*, 38(10), 2011. doi: 10.1029/2011gl047253.
- Cao, A. and Gao, S. S. Temporal variation of seismic *b*-values beneath northeastern Japan island arc. *Geophysical Research Letters*, 29(9), 2002. doi: 10.1029/2001gl013775.
- Corral, Á. Dependence of earthquake recurrence times and independence of magnitudes on seismicity history. *Tectonophysics*, 424(3–4):177–193, 2006. doi: 10.1016/j.tecto.2006.03.035.
- Davidsen, J. and Green, A. Are Earthquake Magnitudes Clustered? Physical Review Letters, 106(10), 2011. doi: 10.1103/phys-revlett.106.108502.
- Goebel, T. H. W., Becker, T. W., Schorlemmer, D., Stanchits, S., Sammis, C., Rybacki, E., and Dresen, G. Identifying fault heterogeneity through mapping spatial anomalies in acoustic emission statistics. *Journal of Geophysical Research: Solid Earth*, 117 (B3), 2012. doi: 10.1029/2011|b008763.
- Gutenberg, B. and Richter, C. F. Frequency of earthquakes in California*. *Bulletin of the Seismological Society of America*, 34(4): 185–188, 1944. doi: 10.1785/bssa0340040185.
- Hainzl, S. Rate-Dependent Incompleteness of Earthquake Catalogs. Seismological Research Letters, 87(2A):337–344, 2016. doi: 10.1785/0220150211.
- Hampton, J., Gutierrez, M., and Matzar, L. Microcrack Damage Observations near Coalesced Fractures Using Acoustic Emission. *Rock Mechanics and Rock Engineering*, 52(10):3597–3608, 2019. doi: 10.1007/s00603-019-01818-4.
- Hardebeck, J. L., Llenos, A. L., Michael, A. J., Page, M. T., and van der Elst, N. Updated California Aftershock Parameters. Seismological Research Letters, 90(1):262–270, 2018. doi: 10.1785/0220180240.
- Hauksson, E., Yang, W., and Shearer, P. M. Waveform Relocated Earthquake Catalog for Southern California (1981 to June 2011). *Bulletin of the Seismological Society of America*, 102(5): 2239–2244, 2012. doi: 10.1785/0120120010.
- Helmstetter, A. Comparison of Short-Term and Time-Independent Earthquake Forecast Models for Southern California. *Bulletin of the Seismological Society of America*, 96(1):90–106, 2006. doi: 10.1785/0120050067.
- Kagan, Y. Y. Short-Term Properties of Earthquake Catalogs and Models of Earthquake Source. *Bulletin of the Seismological Society of America*, 94(4):1207–1228, 2004. doi: 10.1785/012003098.
- Klinger, Y. Relation between continental strike-slip earthquake segmentation and thickness of the crust. *Journal* of Geophysical Research: Solid Earth, 115(B7), 2010. doi: 10.1029/2009jb006550.
- Lei, X. How do asperities fracture? An experimental study of unbroken asperities. *Earth and Planetary Science Letters*, 213(3–4): 347–359, 2003. doi: 10.1016/s0012-821x(03)00328-5.
- Lin, Q., Yuan, H., Biolzi, L., and Labuz, J. F. Opening and mixed mode fracture processes in a quasi-brittle material via digital imaging. *Engineering Fracture Mechanics*, 131:176–193, 2014. doi: 10.1016/j.engfracmech.2014.07.028.
- Lin, Q., Wan, B., Wang, S., Li, S., and Fakhimi, A. Visual detection of a cohesionless crack in rock under three-point bending. *Engineering Fracture Mechanics*, 211:17–31, 2019a. doi: 10.1016/j.engfracmech.2019.02.009.
- Lin, Q., Wan, B., Wang, Y., Lu, Y., and Labuz, J. F. Unifying acoustic emission and digital imaging observations of quasi-brittle fracture. *Theoretical and Applied Fracture Mechanics*, 103:102301, 2019b. doi: 10.1016/j.tafmec.2019.102301.
- Lippiello, E., de Arcangelis, L., and Godano, C. Influence of Time and Space Correlations on Earthquake Magnitude. *Physical Re-*

- view Letters, 100(3), 2008. doi: 10.1103/physrevlett.100.038501.
- Lippiello, E., Godano, C., and de Arcangelis, L. The earthquake magnitude is influenced by previous seismicity. *Geophysical Research Letters*, 39(5), 2012. doi: 10.1029/2012gl051083.
- McLaskey, G. C. and Lockner, D. A. Shear failure of a granite pin traversing a sawcut fault. *International Journal of Rock Mechanics and Mining Sciences*, 110:97–110, 2018. doi: 10.1016/j.ijrmms.2018.07.001.
- Mignan, A. and Woessner, J. Estimating the magnitude of completeness for earthquake catalogs, 2012. doi: 10.5078/CORSSA-00180805. Available at http://www.corssa.org.
- Mizrahi, L., Nandan, S., and Wiemer, S. Embracing Data Incompleteness for Better Earthquake Forecasting. *Journal of Geophysical Research: Solid Earth*, 126(12), 2021. doi: 10.1029/2021jb022379.
- Moradpour, J., Hainzl, S., and Davidsen, J. Nontrivial decay of aftershock density with distance in Southern California. *Journal of Geophysical Research: Solid Earth*, 119(7):5518–5535, 2014. doi: 10.1002/2014jb010940.
- Nandan, S., Ouillon, G., Wiemer, S., and Sornette, D. Objective estimation of spatially variable parameters of epidemic type aftershock sequence model: Application to California. *Journal of Geophysical Research: Solid Earth*, 122(7):5118–5143, 2017. doi: 10.1002/2016jb013266.
- Ogata, Y. and Zhuang, J. Space–time ETAS models and an improved extension. *Tectonophysics*, 413(1–2):13–23, 2006. doi: 10.1016/j.tecto.2005.10.016.
- Pan, X.-H., Xiong, Q.-Q., and Wu, Z.-J. New Method for Obtaining the Homogeneity Index m of Weibull Distribution Using Peak and Crack-Damage Strains. *International Journal of Geomechanics*, 18(6), 2018. doi: 10.1061/(asce)gm.1943-5622.0001146.
- Peng, Z., Vidale, J. E., Ishii, M., and Helmstetter, A. Seismicity rate immediately before and after main shock rupture from high-frequency waveforms in Japan. *Journal of Geophysical Research: Solid Earth*, 112(B3), 2007. doi: 10.1029/2006jb004386.
- Richards-Dinger, K., Stein, R. S., and Toda, S. Decay of aftershock density with distance does not indicate triggering by dynamic stress. *Nature*, 467(7315):583–586, 2010. doi: 10.1038/nature09402.
- Schorlemmer, D. and Woessner, J. Probability of Detecting an Earthquake. *Bulletin of the Seismological Society of America*, 98 (5):2103–2117, 2008. doi: 10.1785/0120070105.
- van der Elst, N. J. *B-Positive*: A Robust Estimator of Aftershock Magnitude Distribution in Transiently Incomplete Catalogs. *Journal of Geophysical Research: Solid Earth*, 126(2), 2021. doi: 10.1029/2020jb021027.
- Veen, A. and Schoenberg, F. P. Estimation of Space–Time Branching Process Models in Seismology Using an EM-Type Algorithm. *Journal of the American Statistical Association*, 103(482): 614–624, 2008. doi: 10.1198/016214508000000148.
- Waldhauser, F. Near-Real-Time Double-Difference Event Location Using Long-Term Seismic Archives, with Application to Northern California. *Bulletin of the Seismological Society of America*, 99(5): 2736–2748, 2009. doi: 10.1785/0120080294.
- Waldhauser, F. and Schaff, D. Regional and teleseismic double-difference earthquake relocation using waveform cross-correlation and global bulletin data. *Journal of Geophysical Research:* Solid Earth, 112(B12), 2007. doi: 10.1029/2007jb004938.
- Wiemer, S. Minimum Magnitude of Completeness in Earthquake Catalogs: Examples from Alaska, the Western United States, and Japan. *Bulletin of the Seismological Society of America*, 90(4): 859–869, 2000. doi: 10.1785/0119990114.

- Woessner, J. Assessing the Quality of Earthquake Catalogues: Estimating the Magnitude of Completeness and Its Uncertainty. Bulletin of the Seismological Society of America, 95(2):684–698, 2005. doi: 10.1785/0120040007.
- Xiong, Q. and Hampton, J. C. Non-Local Triggering in Rock Fracture. *Journal of Geophysical Research: Solid Earth*, 125(11), 2020. doi: 10.1029/2020jb020403.
- Xiong, Q. and Hampton, J. C. A Laboratory Observation on the Acoustic Emission Point Cloud Caused by Hydraulic Fracturing, and the Post-pressure Breakdown Hydraulic Fracturing Reactivation due to Nearby Fault. *Rock Mechanics and Rock Engineering*, 54(12):5973–5992, 2021. doi: 10.1007/s00603-021-02585-x.
- Xiong, Q., Brudzinski, M. R., Gossett, D., Lin, Q., and Hampton, J. C. Seismic magnitude clustering is prevalent in field and laboratory catalogs. *Nature Communications*, 14(1), 2023. doi: 10.1038/s41467-023-37782-5.
- Zambrano Moreno, A. F. and Davidsen, J. Magnitude correlations in a self-similar aftershock rates model of seismicity. *Nonlinear Processes in Geophysics*, 27(1):1–9, 2020. doi: 10.5194/npg-27-1-2020.

The article *The Pattern of Earthquake Magnitude Clustering Based on Interevent Distance and Time* © 2024 by Derreck Gossett is licensed under CC BY 4.0.

SEISMICA | volume 3.2 | 2024